I&EC research
Industrial & Engineering Chemistry Research

Article

pubs.acs.org/IECR

High-Efficiency Simultaneous Oxidation of Organoarsenic and Immobilization of Arsenic in Fenton Enhanced Plasma System

Ping Hu,[†] Yukun Liu,[†] Bo Jiang,[*,†,‡] Xing Zheng,[§] Jingtang Zheng,[*,†] and Mingbo Wu[*,†]

[†]State Key Laboratory of Heavy Oil Processing, China University of Petroleum, Qingdao 266580, Shandong, P.R. China
[‡]Qingdao Technological University, Qingdao 266580, China
[§]Bei Jing Sinen En-Tech Co., Ltd, Beijing 100080, China

Supporting Information

ABSTRACT: Roxarsone (ROX), an organoarsenic compound serving as a common feeding additive, is heavily utilized in the agricultural field and brings about the potential risks of toxic inorganic arsenic contamination in the ambient environment. In this study, the applicability of glow discharge plasma (GDP) for simultaneous oxidation of organoarsenic and immobilization of arsenic is unprecedentedly evaluated. The results show that ROX can be effectively oxidized to inorganic arsenic, and this performance is evidently dependent on energy input. Adding Fe(II) can significantly enhance the oxidation of ROX mainly because of the additional production of $^{\bullet}OH$ via Fenton reaction in GDP, accompanied by which the generated arsenic can be simultaneously immobilized in one process. The immobilization of arsenic can be favorably obtained at pH 4.0−6.0 and Fe(II) concentration ranging from 500 to 1000 μM. On the basis of the mineral compositions and analysis (XRD/FTIR/XPS) of precipitate, a mechanism can be proposed that the oxidation of Fe(II) by H_2O_2 generated in situ in GDP significantly accelerates ROX transformation to the ionic As(V), which can immediately precipitate with Fe(III) ions or be adsorbed on the ferric oxyhydroxides, forming amorphous ferric arsenate-bearing ferric oxyhydroxides. As such, the present study offer a new recipe for rapid decontamination of organoarsenic pollutants, in which the hypertoxic species can be effectively removed from the wastewater.

1. INTRODUCTION

Arsenic is recognized as a hypertoxic and carcinogenic element and prevalently exists as the stable forms of arsenite (As(III)) and arsenate (As(V)) in aquatic environment. In the past decades, the contamination induced by these arsenic species is frequently occurring in natural environments, which primarily resulted from natural processes (e.g., weathering of arsenic-bearing minerals) and arsenic-related anthropogenic activities like metallurgical industries, ceramic industries, pesticides manufacturing industries, and wood preservatives.[1−3,2,3] Thus, arsenic contamination is a significant environmental concern, and its removal attracts serious attention in the area of environmental remediation.

Organoarsenic compounds as a kind of arsenic product, typically exist in a pentavalent oxidation state and are introduced into the environment due to agricultural applications.[2,4] Around the world, aromatic organoarsenic compounds such as roxarsone (3-nitro-4-hydroxyphenylarsonic acid, ROX) are widely used as feed additives, and most of the chemicals are excreted unchanged in the manure.[5] Although these compounds have relatively low toxicity to domestic livestock, they can potentially transform to more toxic and mobile counterpart inorganic species (i.e., As(III) and As(V)) via biotic and abiotic reactions when they are released into aquatic/soil environment.[6] Inevitably, they will contaminate local ground and surface water used for drinking-water supplies and eventually pose risks to human health.[6,7]

Recently, numerous studies have covered the remediation of inorganic arsenic using some conventional technologies (e.g., adsorption, coprecipitation, and coagulation)[8] or to improve the arsenic immobilization efficiency, the developments of some viable oxidation processes, such as chemical oxidation[9] and UV/Fenton[10,11] have been employed for As(III) to As(V) with considering their greatly different mobility. However, unfortunately, the widespread use and environmental threat of organoarsenic species have received much less attention.[2,5,12,13] O'Shea et al.[14] performed detailed adsorption and degradation kinetic studies on the TiO_2 photocatalysis of aromatic organoarsenic, and demonstrated that TiO_2 photocatalytic degradation of ROX leads to its final mineralization to As(V). Nevertheless, as for these established techniques, the formed inorganic arsenic species are still remaining in solution and their removal from waters needs subsequent immobilization processes. In the light of these, it is urgently required to develop environmentally benign and more effective technologies toward simultaneous oxidation of organoarsenic and immobilization detoxification of arsenic.

Glow discharge plasma (GDP), a promising advanced oxidation process, is significantly attractive due to its higher yields of active species including hydroxyl radical ($^{\bullet}OH$) and hydrogen peroxide (H_2O_2), among others, than those expected on the basis of Faraday's law.[15] Owing to the powerful oxidizing ability ($E^0(^{\bullet}OH/H_2O) = 2.8\ V_{NHE}$) and nonselectivity of $^{\bullet}OH$, GDP has been extensively applied for treatment wastewaters containing a variety of organic/inorganic contaminants.[15−18]

Received: March 17, 2015
Revised: July 20, 2015
Accepted: August 2, 2015
Published: August 2, 2015

DOI: 10.1021/acs.iecr.5b01012
Ind. Eng. Chem. Res. 2015, 54, 8277−8286

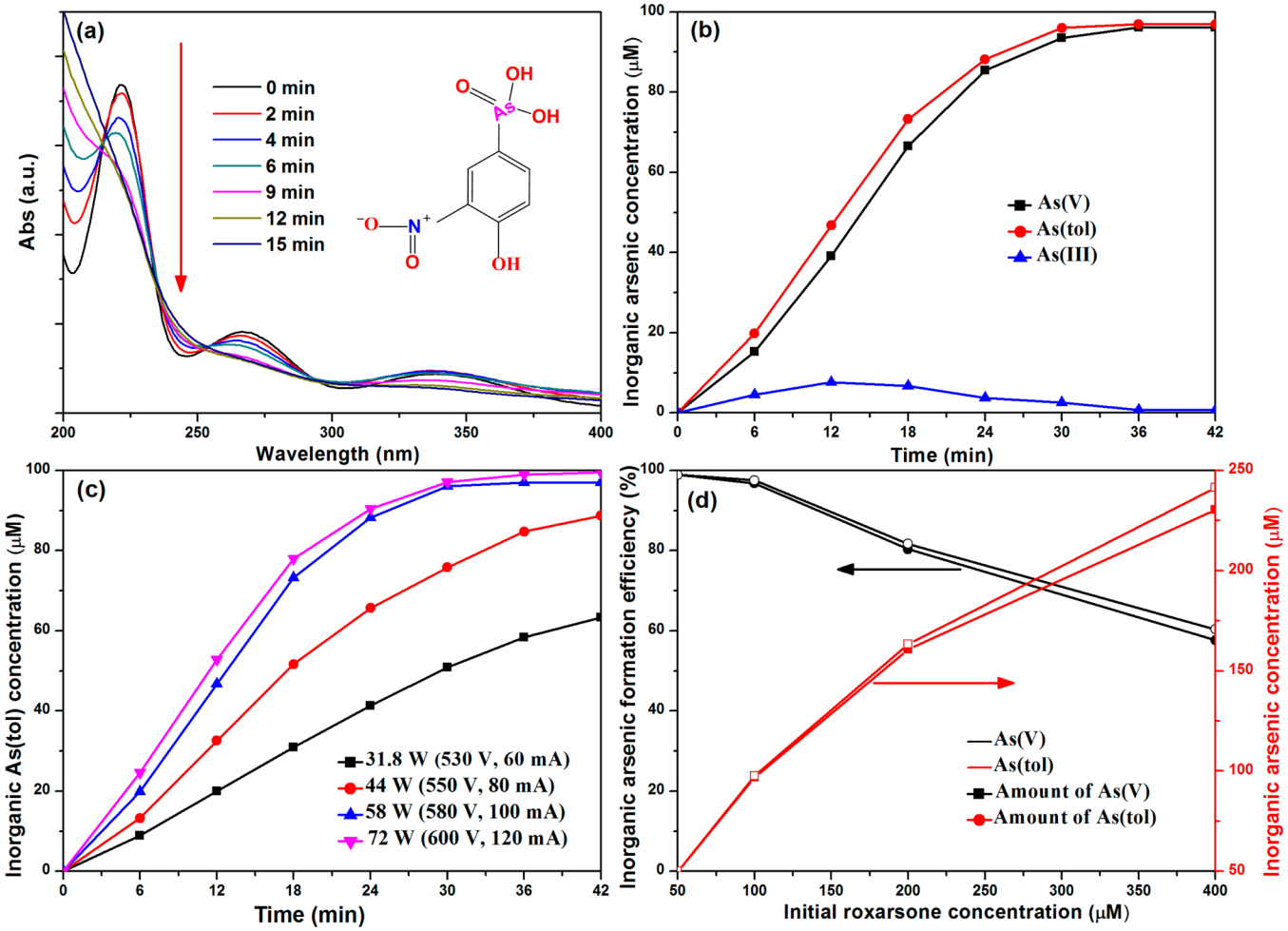

Figure 1. Changes of UV−vis spectra (a) and the formations of inorganic arsenic species (b) in GDP; effect of the input energy on the formation of total inorganic arsenic species (c); effect of initial ROX concentration on the final formations of inorganic arsenic species within 42 min (d) (typical conditions: input energy 58 W, $[ROX]_0$ = 100 μM, pH4.0).

Nevertheless, the application of GDP for the remediation of organoarsenic containing wastewaters, to our knowledge, has not been reported.

Herein, we aimed at inspecting the flexibility of GDP for organoarsenic oxidation and simultaneous immobilization of hypertoxic inorganic arsenic in one process. ROX was selected as a model target in this study with considering its common utilization.[4,5] The oxidation performance of ROX was investigated first in GDP, and the effects of electrical discharge and initial concentration were subsequently examined. In addition, the impacts of solution pH and initial Fe(II) concentration on oxidization ROX and simultaneous immobilization of the produced inorganic arsenic were also estimated. Furthermore, radical quenching and complexing agents addition experiments were carried out to clarify the underlying mechanism of ROX pollutant remediation in GDP coupled with Fenton reaction system.

2. EXPERIMENTS

2.1. Materials. Roxarsone (ROX, 98%) was purchased from TCI Scientific. Sodium arsenite ($NaAsO_2$, 97%) and ferrous sulfate were supplied by Xiya Reagent and Sinopharm Chemical Reagent Co. Ltd., respectively. All chemical reagents were used without further purification. UltraPure water (18.2 MΩ·cm) was used for all experiments. The stock solutions of ROX (5 mM) was prepared by dissolving appropriate amounts of ROX. Fe(II) base solution (10 mM) was prepared by dissolving $FeSO_4$ in 1 mM H_2SO_4 with adding a spot of reduced iron powder.

2.2. Experimental Procedure. The experimental apparatus consisted of a DC high voltage power supply and a reactor, which is similar to that described elsewhere,[17] as shown in Figure S1. All working solutions were freshly prepared before use by diluting the stock Na_2SO_4 electrolyzing solution, and solution pH was adjusted to the desired values with diluted solution of H_2SO_4 or NaOH. Typically, 150 mL of argon-purged Na_2SO_4 solution (conductivity 3.4 mS cm^{-1}, pH 4.0) with 100 μM ROX was treated by GDP (580 V/100 mA). The bulk solution in the reaction vessel was maintained at 298 ± 2 K by running cooling water and was magnetically stirred. The depth of the electrode immersed in the solution was carefully adjusted to stabilize the input current and voltage with deviation less than ±3%.

In the cases of adding Fe(II), samples of the suspension were withdrawn at various time intervals and immediately filtrated through PTFE microporous filtering film (pore diameter 0.25 μm), and then the concentrations of residual As and Fe in the filtrate were analyzed. To determine mineral compositions of precipitations in this process, the precipitation was separated from solution via vacuum suction filtration and subsequently

DOI: 10.1021/acs.iecr.5b01012
Ind. Eng. Chem. Res. 2015, 54, 8277−8286

redissolved in H_2SO_4 solution (pH 2.0, 100 mL) for the measurement of arsenic and iron species.[19] All experiments were conducted in duplicate, and the relative error was less than 5%.

2.3. Analysis. The conductivity and pH of solution were determined by conductivity meter (DDS-307A) and pH meter (PHS-3C), respectively. UV−vis spectra for ROX was collected using a spectrophotometer (UV-3000, MAPADA). Inorganic arsenic (As(V)) concentration was measured by the developed molybdate-based method, with a detection limit of 0.03 μM.[20] The concentration of ferrous ion was spectrophotometrically determined at the wavelength of 510 nm using a modified phenanthroline method.[21] H_2O_2 generated in plasma system was detected by a spectro photometrical method using titanyl reagent.[22] The total organic carbon (TOC) was calculated by the TOC analyzer (Liqui TOC-II, Elementar).

Based on eq 1, $^{\bullet}$OH produced in GDP was estimated by employing coumarin (1.0 mM) as a selective trap $^{\bullet}$OH. The fluorescence intensity of 7-hydroxycoumarin was determined by fluorescence spectrophotometer (F97PRO, Lengguang Tech.) at $\lambda_{excitation}$ = 322 nm and $\lambda_{emission}$= 455 nm).[23]

$$\text{coumarin} + {}^{\bullet}\text{OH} \rightarrow 7-\text{hydroxycoumain} \qquad k_1 = 2 \times 10^9\ \text{M}^{-1}\ \text{s}^{-1} \tag{1}$$

The precipitates formed in GDP/Fenton process were washed repeatedly with ultrapure water and dried under reduced pressure (133 Pa) at 50 °C for 40 h. The abrasive powder was characterized by FTIR (Thermo Nicolet NEXUS), XRD (X' Pert Pro MPD, Holland), and XPS (PHI5000 Versa Probe, ULVAC-PHI, Japan).

3. RESULTS AND DISCUSSION

3.1. Conversion of ROX in GDP System. It is known that UV−vis spectra can indirectly reflect the molecule structures of some organic pollutants.[6] Thus, to inspect the oxidation of ROX in GDP, the UV−vis spectra changes of ROX were monitored as a function of reaction time in Figure 1a. As for virgin ROX solution, the absorption bands at 340/220 and 270 nm mainly originate from the nitro-group and hydroxyl group on aromatic ring, respectively.[6,24] When ROX solution was exposed to GDP, the intensity of these absorption bands gradually decreased to the negligible extent within 15 min. It indicated that the nitro-group and hydroxyl-group on aromatic ring were effectively destroyed in plasma treatment. In spite of no corresponding absorption band for arsenic group in ROX molecule, according to Figure 1b, arsenic group can be also disrupted from ROX molecules, and after 42 min GDP treatment, approximately 97% of ROX was transformed into inorganic arsenic, mainly present as As(III) and As(V).

It has been well illustrated that $^{\bullet}$OH is a strong oxidant with high oxidation potential up to 2.8 V_{NHE} and dominates the destruction of hazardous organics in GDP.[15,25] Its reaction with organics can be mainly differentiated into three different pathways: abstraction of hydrogen atom, electrophilic addition to unsaturated bond, and electron transfer.[15] As regards ROX degradation, due to its property of electron-rich in ROX molecule, the As−C bond is highly vulnerable to the attack of $^{\bullet}$OH via electrophilic addition of hydroxyl radical leading to the cleavage of the As−C bond.[2,26] In this process, As(IV), an intermediate of the homolytic As(V)−C bond cleavage, can readily disproportionate to yield 1:1 ratio of As(III) and As(V).[26] Subsequently, the generated As(III), as an electron donator, can be rapidly and concurrently oxidized to As(V) by $^{\bullet}$OH.[27] Thus, the concentration of As(III) is much lower than As(V) in solution, and As(V) is the eventual product for ROX oxidation. As discussed above, the oxidation of organoarsenic compounds can transform arsenic from organic form to inorganic form and the formed inorganic arsenic can availably reflect the oxidation extent of organoarsenic. Therefore, the concentration of formed inorganic arsenic will be used as a credible index mirroring the ROX oxidation in GDP.

Energy input is a key parameter for the onset of GDP.[15] In this experiment, the effect of input energy on ROX oxidation was investigated from 31.8 (530 V/60 mA) to 72 W (600 V/120 mA). Figure 1c depicts that increasing the applied energy greatly accelerated the oxidation of ROX. Specifically, approximately 100 μM inorganic As(tol) was produced at the input energy of 72 W within 42 min, which was much larger than 63 μM inorganic As(tol) generation in the case of 31.8 W. The enhanced ROX oxidation can be attributed to the fact that higher energy was favorable for larger amount of $^{\bullet}$OH generation, which can be evidenced by the fluorescence intensity of produced 7-hydroxycoumarin in Figure S2a.

In the plasma-generating process, the formed $^{\bullet}$OH exhibits short-lived (lifetime: 3.7×10^{-9} s), and thus the concentrated $^{\bullet}$OH in plasma generating zone probably vanishes via the dimerization reaction with the formation of H_2O_2, a long-lived plasma product.[28] As presented in Figure S2b, with increasing the input energy from 31.8 to 72 W, the formation rate of H_2O_2 increased from 6.9 to 14.4 mg L^{-1} min^{-1}, which averagely corresponds to 0.81 mol H_2O_2 (mol electron)$^{-1}$ much higher than that expected from Faraday's law (0.5 mol H_2O_2 (mol electron)$^{-1}$). In addition, we can observe no significant concentration reduction of H_2O_2 for ROX-bearing solution comparing with that in the blank test in Figure S3. It highlights that though H_2O_2 is abundantly produced in GDP and owns relatively high oxidation potential ($E^0(H_2O_2/H_2O)$ = 1.77 V), the contribution of H_2O_2 to ROX oxidation was negligible.

Figure 1d shows that higher initial concentration resulted in lower inorganic arsenic formation efficiency but a larger absolute amount of organic arsenic oxidation. Specifically, when the initial ROX concentration was 400 μM, only approximately 60% inorganic arsenic (approximately 240 μM) can be produced within 42 min. It can be ascribed to the fact that the higher initial concentration, the stronger the competition between the initial reactant and the intermediate products with active species.

3.2. Oxidation of ROX and Immobilization of Arsenic in GDP/Fenton Process. As mentioned above, H_2O_2 can be substantially generated in situ by GDP and it is a mild oxidant impotent to the oxidation of pollutant. But the presence of H_2O_2 increases the collective oxidbillity of the plasma and significantly affects plasma chemistry. For example, H_2O_2 can be used as an alternative source of $^{\bullet}$OH via iron-based catalytic reactions (i.e., Fenton reaction).[15] Besides, the iron ion, as a cost-effective flocculant, is widely utilized for arsenic immobilization from high arsenic-contaminated wastewater.[29,30] Thus, in efforts to enhance the oxidation of ROX and immobilization of inorganic arsenic, addition of iron ions in GDP is an attractive alternative arising from the fact that the added iron ions can not only catalytically transform H_2O_2 into $^{\bullet}$OH via Fenton reaction (eqs 2,3) but also simultaneously immobilize inorganic arsenic forming precipitation.

$$H_2O_2 + \text{Fe(II)} \rightarrow {}^{\bullet}\text{OH} + {}^{-}\text{OH} + \text{Fe(III)} \qquad k_2 = 70\ \text{M}^{-1}\ \text{s}^{-1} \tag{2}$$

DOI: 10.1021/acs.iecr.5b01012
Ind. Eng. Chem. Res. 2015, 54, 8277−8286

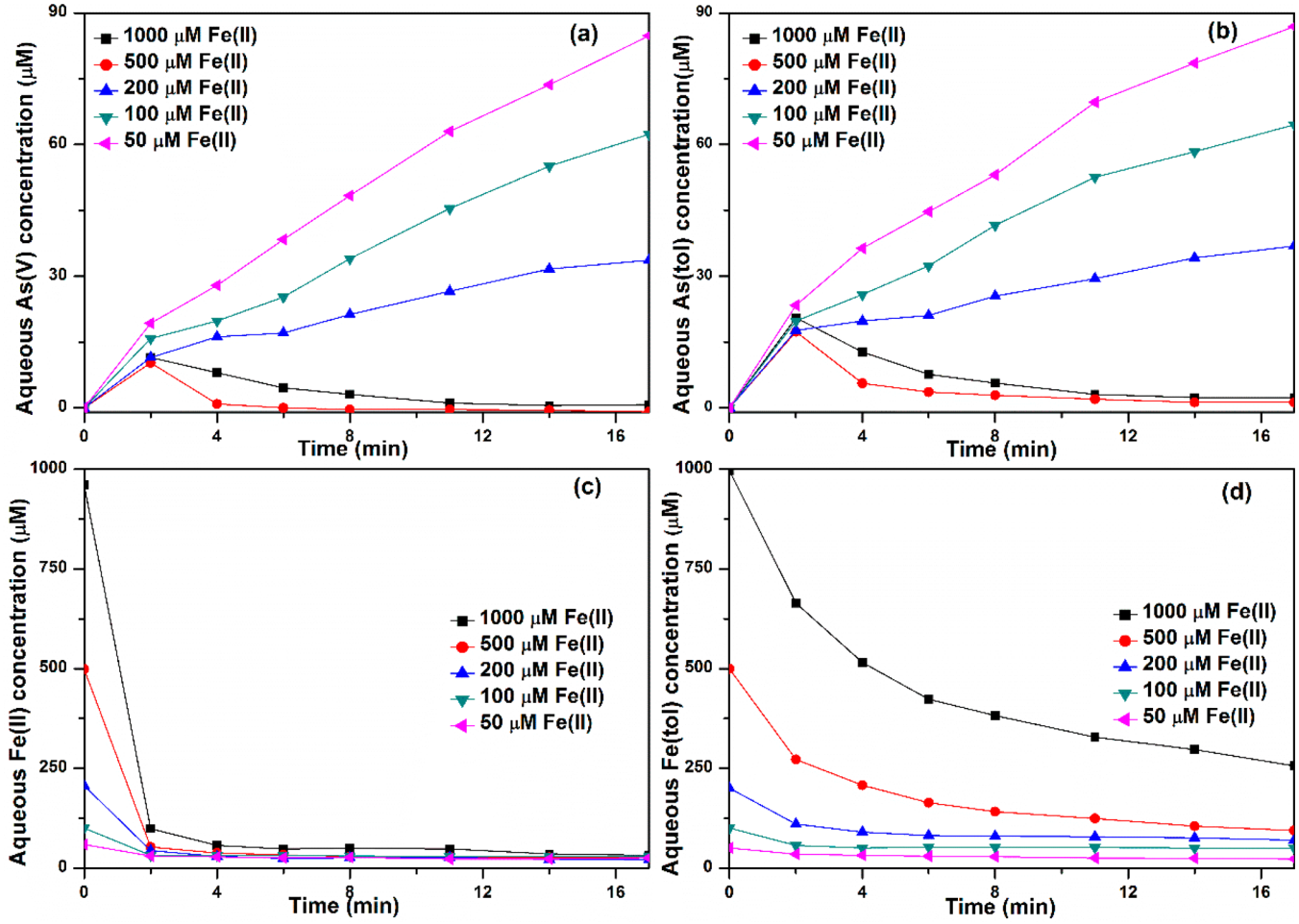

Figure 2. Effect of Fe(II) concentration on inorganic arsenic formation, arsenic immobilization, Fe(II) oxidation, and iron immobilization in GDP (input energy 58 W, $[ROX]_0$ = 100 μM, pH 4.0).

$$H_2O_2 + Fe(III) \rightarrow Fe(II) + OOH^- + H^+ \qquad k_3 = 0.01\ M^{-1}\ s^{-1} \tag{3}$$

In this section, Fe(II) addition with a concentration from 50 to 1000 μM was studied as shown in Figure 2. When 50 μM Fe(II) was added in GDP, Fe(II) can be rapidly oxidized to Fe(III) within 2 min, as depicted in eq 2, in which much additional •OH was produced via Fenton reaction, as illustrated in Figure 2c. This can be validated by fluorescence spectra in Figure 3. Consequently, in this case, ROX oxidation to inorganic arsenic was significantly enhanced in GDP/Fenton process as depicted in Figure 2a,b. For example, approximately 88 μM aqueous inorganic arsenic was generated in the presence of 50 μM Fe(II) within 17 min, which was larger than 69 μM inorganic arsenic formation in the absence of Fe(II) within 18 min. Besides, as exhibited in Figure 3, the increased production of •OH can be further improved by increasing the concentration of Fe(II) from 50 to 500 μM. However, the detected aqueous inorganic arsenic concentration was decreased with increasing Fe(II) concentration above 50 μM as shown in Figure 2b. In these processes, we can observe the gross of turbidities in solution variation from negligible white gray to considerable brown with increasing Fe(II) addition from 50 to 1000 μM (Figure S4). Thus, the unmatched results of •OH yield and aqueous inorganic arsenic concentration are probably attributed to the formation of arsenic-bearing precipitate with the presence of relatively large Fe(II) concentration in GDP.

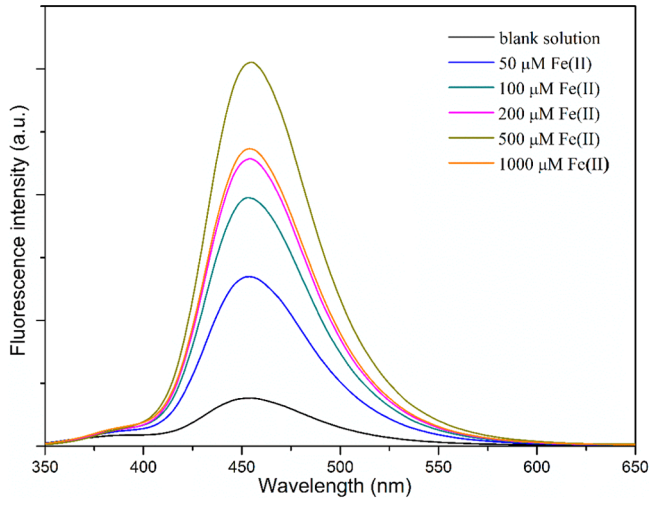

Figure 3. Fluorescence intensity of 7-hydroxycoumarin produced in various solutions mediated GDP system at 4.0 min (input energy 58 W, $[ROX]_0$ = 100 μM, pH 4.0).

Table S1 shows the constitution of precipitates formed in the ROX oxidation process mediated by GDP/Fenton. For 50 μM Fe(II), only a small amount of precipitate was formed with

DOI: 10.1021/acs.iecr.5b01012
Ind. Eng. Chem. Res. 2015, 54, 8277−8286

inorganic arsenic immobilization efficiency of approximately 12%. Higher Fe(II) addition in GDP could induce and favor higher arsenic immobilization efficiency. In the case of adding 500 μM Fe(II), aqueous arsenic and iron continuously decreased in the whole treatment process with relatively high immobilization efficiency of approximately 86% and 81%, respectively, after 17 min. Thus, the performance of inorganic arsenic immobilization is strongly dependent on the initial iron addition. Besides, it is clear that inorganic As(V) and Fe(III) are the main mineral compositions of the precipitates for various Fe(II) addition in Table S1. The effect of Fe(II) addition on the immobilization efficiency of iron ions was found to be similar to that of arsenic species indicated by Figure 2d and Table S1. Taken together, in these processes, we can infer that the formed ionic As(V) immediately coprecipitated with Fe(III) ions as ferric arsenate or was adsorbed on the ferric oxyhydroxides, which was produced via the hydrolysis reactions of aqueous Fe(III) ions.[31] It is known that ferric arsenate has a higher saturation index than that of ferric oxyhydroxide in a mildly acidic condition and per Stranski's rule.[32] Thus, in these processes, ferric arsenate should be formed preferentially, after which ferric oxyhydroxide would be formed, on which the residual arsenic was adsorbed.[29] Robins et al.[30] found the solubility of the arsenic-bearing precipitates decrease with increasing Fe/As molar ratio. In addition, based on the mineral compositions of precipitations, it was calculated that the ratio of solid As/solid Fe was high, up to 0.68 for initial Fe(II) concentration of 100 μM and reduced significantly by raising Fe(II) addition. These results suggest that aqueous Fe(III) ions with relatively low concentration have an affinity toward reaction with As(V) rather than the formation of ferric hydroxide.

3.3. Effect of pH. Because both the accumulation of ferric oxyhydroxides and formation of ferric arsenate precipitation are closely related with solution pH, a series of experiments were carried out in pH range of 2.5−6.0. As depicted in Figure 4, at pH 2.5, aqueous inorganic As(tol) concentration can rapidly reach approximately 88 μM within 8 min, whereas a negligible amount of As(V) was detected at a pH value above 4.0. As to Fe(tol) species, its immobilization efficiency was facilitated by decreasing solution acidity with pH range of 2.5−6.0 (see Figure 4 and Table 1). Similar variation tendency induced by solution pH can be also observed for aqueous As(V) and Fe(III) in Figure S5. According to the constitution of precipitates in Table 1, it can be found that the inorganic As(tol) (aqueous + solid) formation efficiency decreased from 95% to 65% within 17 min with pH increasing from 2.5 to 6.0.

These results may be attributed to the reaction scheme that additional formation of $^{\bullet}$OH via traditional Fenton reaction was inhibited at relatively low acidity solution.[10] Conversely, the slight acidity was in favor for the immobilization of arsenic and iron species. For example, substantial iron ions precipitated at pH 4.0−6.0, and the As(V) can be immediately immobilized once it was produced in GDP/Fenton, which leads to the minor residue of iron or arsenic species in aqueous solution. As shown in Table 1, at relatively low pH (i.e., 2.5 and 3.0), arsenic immobilization efficiency was evidently retarded because of the high solubility of amorphous ferric arsenate precipitates at relatively strongly acidic solution. Based on the thermodynamic properties of scorodite used in the construction of Eh−pH diagrams from the previous literatures, a large stability field of scorodite was formed in As−Fe system under acidic and neutral pH with oxidizing conditions (in Figure S6).[33] It indicates that the addition of Fe into the As−O−H system results in significantly decreased arsenic mobility under extremely oxidizing and low pH conditions and neutral pH conditions.

As discussed above, the strong acid condition can significantly favor the ROX oxidation, while the weak acid can provide the more desired condition for arsenic immobiliza-

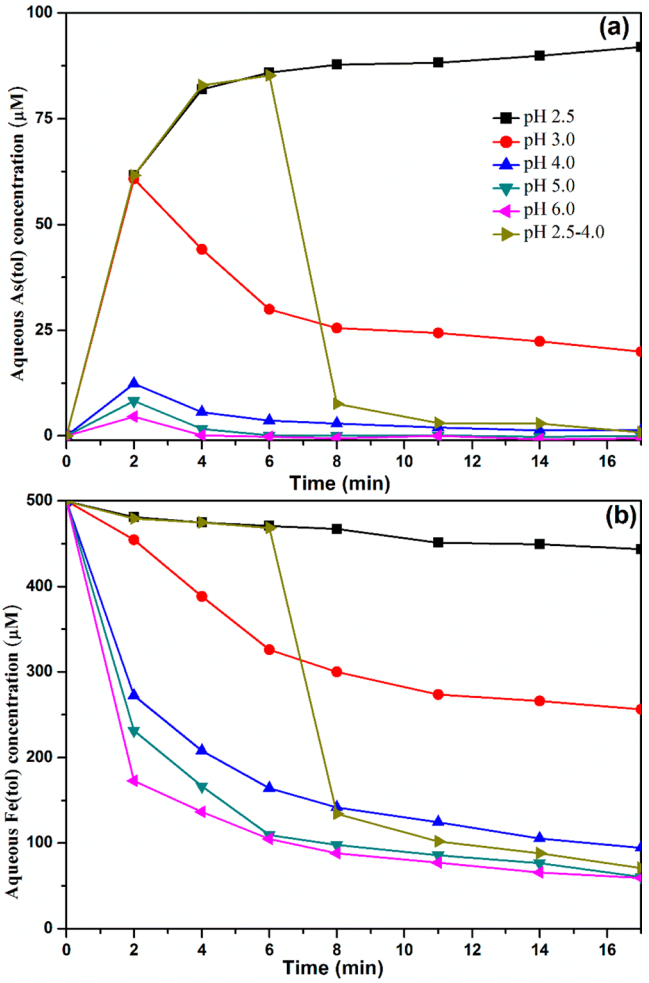

Figure 4. Effect of solution pH on the conversion of ROX and the immobilizations of inorganic arsenic and iron (input energy 58 W, $[ROX]_0$ = 100 μM, $[Fe(II)]_0$ = 500 μM).

Table 1. Mineral Composition of Precipitates Produced in GDP/Fenton Process Mediated by Various pH after a 17 min Treatment (Input Energy 58 W, $[ROX]_0$ = 100 μM, $[Fe(II)]_0$ = 500 μM, pH 4.0)

initial pH	2.5		3.0		4.0	
	solid	solution	solid	solution	solid	solution
$As(V)/As_{ini}$	1%	87%	67%	12%	79%	3%
$As(t)/As_{ini.}$	3%	92%	70%	14%	85%	4%
$Fe(II)/Fe_{ini.}$	7%	13%	14%	21%	20%	24%
$Fe(t)/Fe_{ini.}$	18%	83%	51%	49%	81%	17%
	5.0		6.0		2.5−4.0	
	solid	solution	solid	solution	solid	solution
$As(V)/As_{ini}$	57%	3%	56%	2%	82%	4%
$As(t)/As_{ini.}$	63%	4%	62%	3%	90%	4%
$Fe(II)/Fe_{ini.}$	18%	10%	15%	6%	7%	4%
$Fe(t)/Fe_{ini.}$	83%	14%	85%	12%	89%	6%

DOI: 10.1021/acs.iecr.5b01012
Ind. Eng. Chem. Res. 2015, 54, 8277−8286

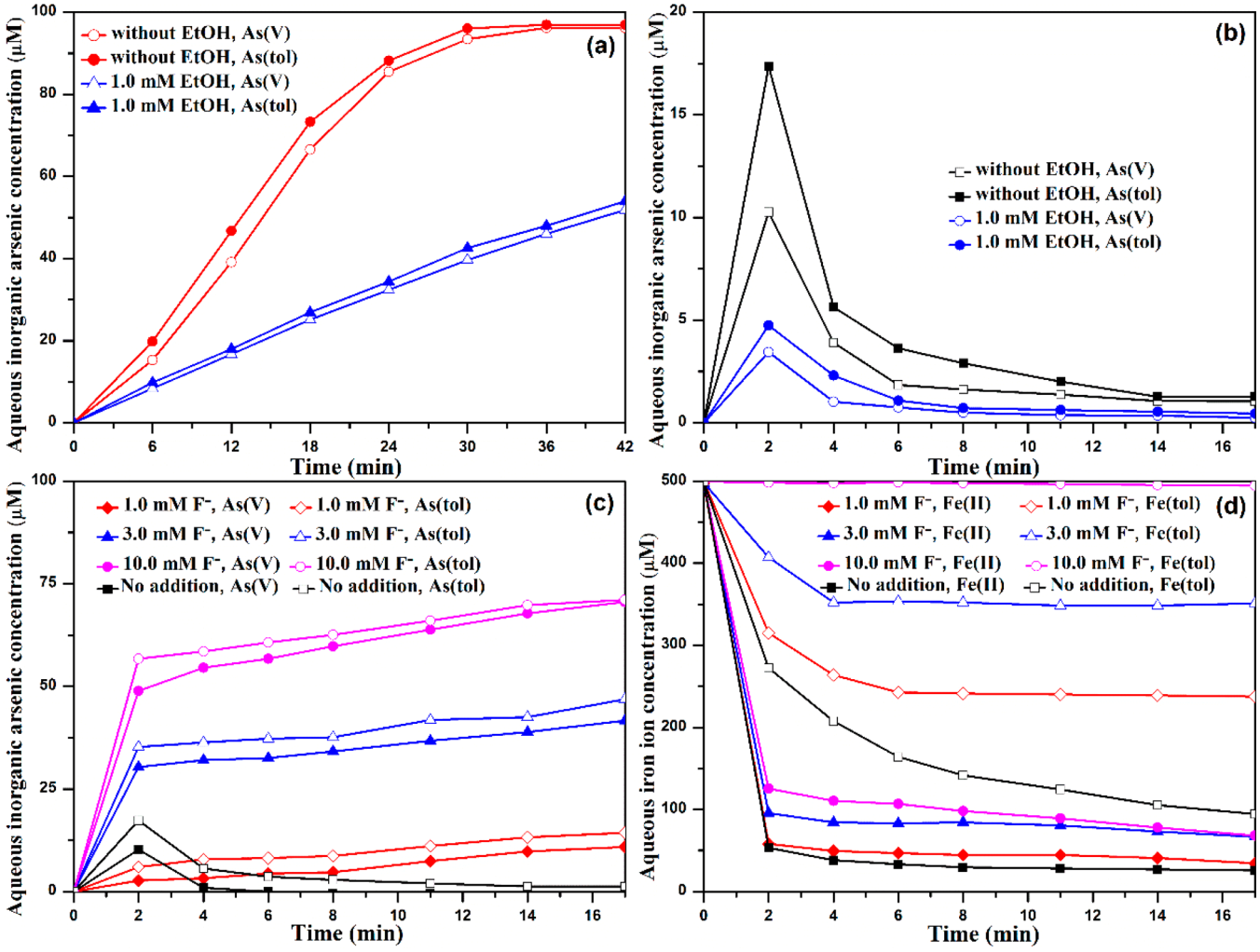

Figure 5. Effect of ethanol addition on the formation of inorganic arsenic (a) in GDP and on the immobilization of inorganic arsenic (b) in GDP/Fenton; effect of fluorine on addition on inorganic arsenic formation and the immobilization of arsenic (c) and iron (d) in GDP-Fenton (input energy 58 W, $[ROX]_0$ = 100 μM, $[Fe(II)]_0$ = 500 μM, pH 4.0).

tion. Thus, the process at a fixed pH may not provide the best of both worlds, with an effective oxidation of ROX and preferable immobilization of the produced inorganic arsenic. Accordingly, a more effective strategy was proposed to balance the ROX oxidation and arsenic immobilization in one process, in which ROX oxidation was proceeded at highly acidic environment in earlier stage and then was switched to arsenic immobilization via elevating the solution pH to a preferable value. An attractive result as expected can be obtained that not only the formation of inorganic arsenic significantly enhanced to 95 μM but the immobilization efficiency of arsenic and iron ion also increased to approximately 89% and 90%, respectively, under the condition that solution pH 2.5 before 6 min and then instantaneously elevating solution pH to 4.0 at latter 11 min in GDP/Fenton.

3.4. Effect of Hydroxyl Radical Scavenger and Complexing Agent. To verify the contribution of $^{\bullet}$OH to ROX oxidation, quenching experiments using ethanol (EtOH) as a $^{\bullet}$OH scavenger were conducted. The results in Figure 5a indicated that the added EtOH evidently retarded the ROX oxidization and finally inhibited inorganic arsenic formation. Specifically, only approximately 50% of ROX was oxidized to inorganic arsenic with the presence of 1 mM EtOH in sole GDP system. Furthermore, more intensive inhibition of ROX oxidation induced by 1 mM EtOH can be observed in GDP coupled with Fenton system (in Figure 5b). For example, the inorganic As(tol) formation and its immobilization were significantly reduced from approximately 90% and 85% to 17% and 14% (not given in the tables), respectively, with adding 1 mM EtOH in GDP/Fenton.

It is known that the produced $^{\bullet}$OH is highly reactive and mainly confined in the plasma-generating zone due to its short diffusion distance (approximately 6 nm) in GDP.[35] Thus, as for ROX, its oxidation is probably limited within the outer plasma zone in the sole GDP system. In this process, the unused $^{\bullet}$OH transforms to the stable H_2O_2 via dimerization and then diffuses into the bulk solution. Thus, when adding Fe(II) in GDP, the pervasive H_2O_2 in solution can be an alternative source of homogeneous $^{\bullet}$OH via Fenton reactions, leading to a synergistic effect in ROX oxidation to inorganic arsenic. In GDP, small-molecular EtOH not only can permeate into the vicinity of plasma zone but also can effectively scavenge $^{\bullet}$OH. Therefore, its presence in the sole GDP system can evidently interrupt the oxidation of ROX. But in the GDP/Fenton system, EtOH simultaneously scavenges $^{\bullet}$OH produced in both heterogeneous plasma zone and homogeneous solution, which was coincident with the fluorescence intensity of 7-hydroxycoumarin in Figure S7.

DOI: 10.1021/acs.iecr.5b01012
Ind. Eng. Chem. Res. 2015, 54, 8277−8286

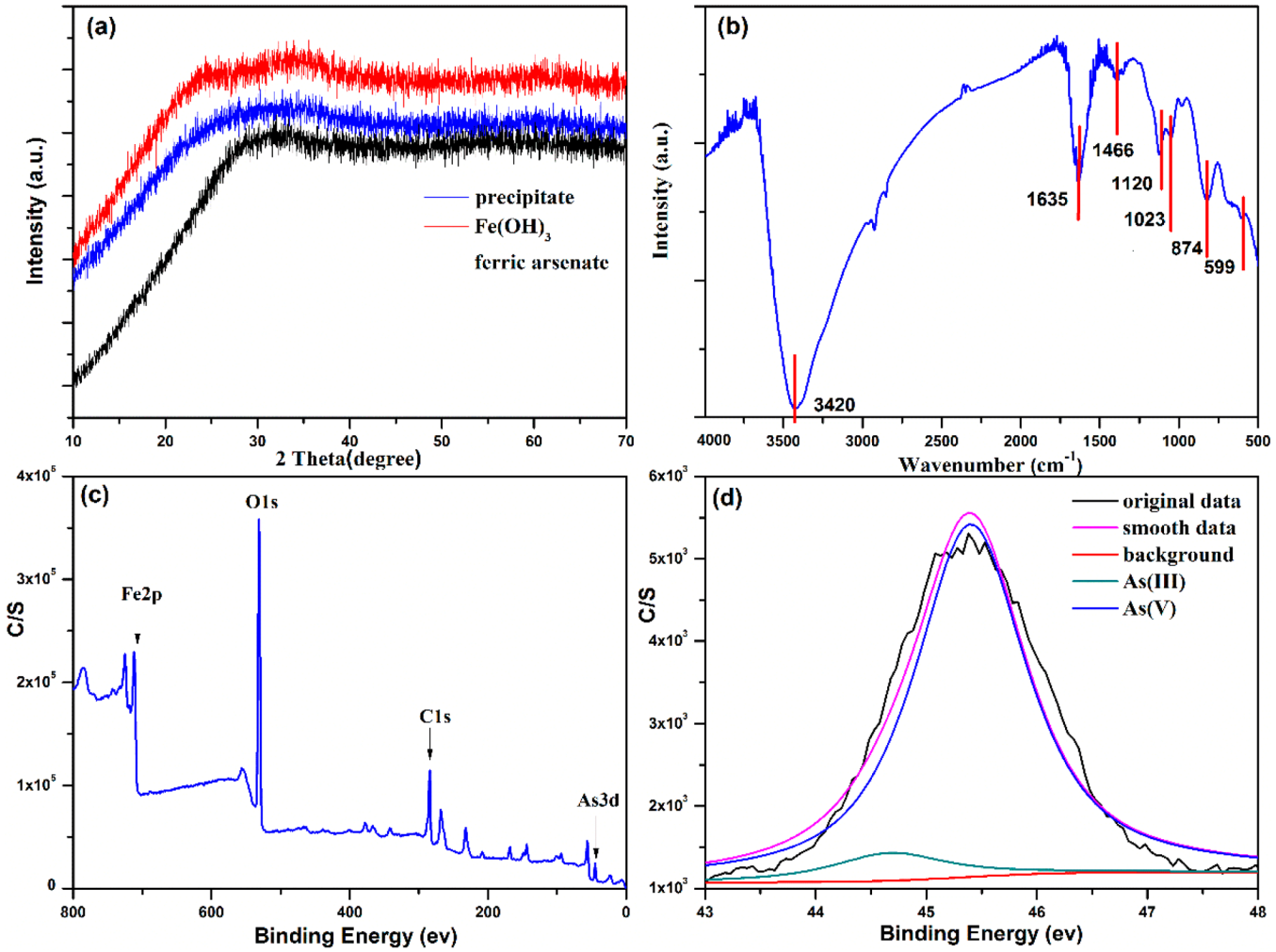

Figure 6. X-ray diffraction pattern (a), FTIR (b), the survey scan XPS spectra (c), and As 3d XPS spectra (d) of precipitate generated during GDP-Fenton process (input energy 58 W, $[ROX]_0$ = 100 μM, $[Fe(II)]_0$ = 500 μM, pH 4.0).

Figure 5c, d illustrate that fluorion can effectively restrain the immobilizations of iron and arsenic, but it has a lesser influence for inorganic arsenic formation. For example, when fluorion addition was 10 mM in GDP/Fenton, the formation of inorganic As(V) and As(tol) were 70 and 71 μM, respectively, without the formation of precipitation (negligible immobilization of iron species). Fluorion can effectively form a complex with the Fe(III) ion, and thus, H_2O_2 may not replace a coordinated ligand in Fe(III)−F complex for Fe(II) regeneration (see eq 3). Thus, the formation $^{\bullet}$OH via Fenton reaction can be interrupted, leading to the less $^{\bullet}$OH formation compared with the case of free fluorion, and this can be proved by decreased 7-hydroxycoumarin fluorescence intensity in Figure S8. In addition, the formed Fe(III)−fluorion complex can stabilize iron species in solution at a larger pH range and hence greatly inhibited the formation of ferric hydroxide precipitate and the production of ferric arsenate.

3.5. Characterization of the Precipitate. The precipitate was analyzed by FTIR, XRD, and XPS to identify its composition and the chemical state present. Figure 6a shows that the product of arsenic-bearing precipitate was poorly crystalline, which makes it difficult to characterize their arsenate phases using XRD. According to previous reports, the coprecipitated Fe(III)−As(V) solid at acidic pH usually consists of poorly crystalline ferric arsenate and arsenate-adsorbed ferrihydrite.[36,37] The FTIR absorption pattern of the precipitate was analyzed in Figure 6b. Broad and strong peak at 3420 cm^{-1} is supposed to be the OH stretching band. The absorption bands at 1637 and 1466 cm^{-1} may be ascribed to the H−O−H bending vibration and ∂(OH), respectively.[38] The peak at 874 cm^{-1} observed can be assigned to the As(V)−O stretching, whereas a negligible peak was observed at 795 cm^{-1} for As(III)−O in the precipitate.[39]

Figure 6c presents the wide-scan XPS spectrum containing surface composition of sediment, suggesting that the precipitate consists primarily of Fe, O, and As, while a small amount of C was detected, which might be originated from organic arsenic or intermediate that was adsorbed on the surface of precipitate.[40] The Fe 2p spectrogram (Figure S9) shows distinct peaks corresponding to the binding energy of Fe $2p_{3/2}$ (711.5 eV) and Fe $2p_{1/2}$ (724.8 eV) of oxidized iron.[41] In addition, the iron signal appears at ∼711.5 eV, which is typical of iron oxy-hydroxides.[42] As reported, the binding energy of As 3d for As(III) and As(V) in arsenic oxides is commonly 44.3−44.5 eV and 45.3−45.6 eV, respectively.[43] In this study, the As 3d spectra (Figure 6d) could be fitted with two components of binding energies at 44.6 and 45.2 eV, corresponding to As(III) and As(V), respectively. Besides, the quantitative analysis based on the area ratio of two overlapped peaks shown that 92% of As in the solid existed as As(V). These results indicated that As(V)

DOI: 10.1021/acs.iecr.5b01012
Ind. Eng. Chem. Res. 2015, 54, 8277−8286

is dominating as As(V) has an affinity toward reaction with Fe(III) forming ferric-arsenate or easily adsorbed on the ferric oxyhydroxides, which is consistent with the results in Table S1.

3.6. Changes of TOC during GDP Process. TOC is an important indicator of water contamination.[6] Thus, the reduction efficiencies of TOC in GDP and GDP/Fenton system were compared in Figure 7. It has been proved that the

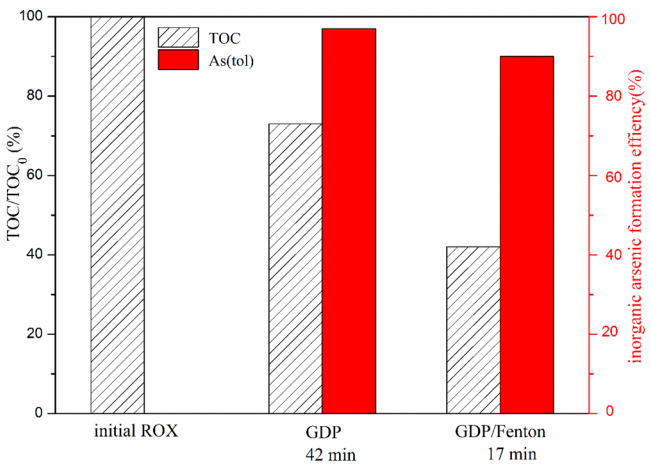

Figure 7. Changes of TOC in ROX solution under various treatment conditions (input energy 58 W, $[ROX]_0$ = 100 μM, $[Fe(II)]_0$ = 500 μM, pH 4.0).

ROX oxidation efficiency was approximately 97% within 42 min in GDP, whereas reduction of TOC was not significant (only 27.4%), indicating that some organic intermediate products were not completely mineralized during GDP. However, in the presence of 500 μM Fe(II), 58% TOC disappeared in only 17 min. This observation suggests that accompanied by the formation of inorganic arsenic, ROX can be mineralized to H_2O and CO_2 in GDP coupled with Fenton process.

3.7. Energy Efficiency. Interest in the utilization of advanced oxidation processes (AOPs) for the treatment of wastewater and the destruction of chemical waste has increased enormously in the last several decades, mainly because of environmental compatibility and high removal efficiency.[44] The organoarsenic degradation efficiency may be better illustrated by the amount of organic decomposed per unit of energy (yield). Table 2 presents the detailed data of energy yields under various conditions. Although appreciable organoarsenic oxidation efficiency can be obtained using these technologies, energy efficiencies were not only less than GDP-Fenton system but also failed to simultaneously immobilize arsenic from waters. Consequently, GDP coupled with the Fenton process was a more efficient strategy for simultaneous oxidation of organoarsenic and immobilization of arsenic.

4. CONCLUSION

In this study, an environmental benign process GDP can efficiently oxidize organoarsenic to inorganic arsenic, which can be further and significantly enhanced with the addition of iron ions as both Fenton catalyst and flocculant. The synergistic effect in $^{\bullet}OH$ production in GDP/Fenton system guarantees the high performance in oganicarsenic oxidation and the inorganic arsenic production. In this process, the formed ionic As(V) rapidly coprecipitated with Fe(III) ions or was adsorbed on the ferric oxyhydroxides with the formation of amorphous ferric arsenate-bearing ferric oxyhydroxides. Generally, the GDP coupled with the Fenton process is an efficient strategy for organoarsenic oxidation and arsenic immobilization, holding promise for the remediation of organicarsenic wastewater.

■ ASSOCIATED CONTENT

Supporting Information

The Supporting Information is available free of charge on the ACS Publications website at DOI: 10.1021/acs.iecr.5b01012.

Experimental details and supplemental data as noted in the text (PDF)

■ AUTHOR INFORMATION

Corresponding Authors

*E-mail for J.-T.Z.: jtzheng03@163.com. Tel.: +86 86984637. Fax: +86 546 8395190.

*E-mail for M.-B.W.: wumb@upc.edu.cn.

*E-mail for B.J.: bjiang86upc@163.com.

Notes

The authors declare no competing financial interest.

■ ACKNOWLEDGMENTS

This work is financially supported by National Natural Science Foundation of China (Nos. 21376268, 21176260, 51172285, and 51372277), State Key Development Program for Basic

Table 2. Comparisons of Organoarsenic Oxidation Efficiency by Using Different Advanced Oxidation Technologies

sample no.	AOPs	other parameters	organoarsenic (μM)	degradation efficiency	removal efficiency	energy efficiency (g/kw h)
1	GDP (present work)	input energy 58 W, pH = 4.0, V = 150 mL, T = 42 min	Roxarsone 100	97%	----	0.097
2	GDP-Fenton (present work)	input energy 58 W, $[Fe(II)]_0$= 500 μM, pH = 4.0, V = 150 mL, T = 17 min	Roxarsone 100	100%	86%	0.24
3	photocatalytic[43]	UV 16 W, 2g/L TiO_2, 315 nm > λ > 280 nm, pH = 4.0, V = 150 mL, T = 480 min	Roxarsone 95	97.9%	16.9%	0.038
4	photo-oxidation[2]	UV 14 W, λ = 254 nm, $[H_2O_2]_0$ = 18.3 g/L T = 160 min, pH = 2.24 V = 100 mL	p-arsanilic acid, 8.9×10^3	100%	50%	0.46
5	UV/O_3[12]	UV 15 W, $[O_3]_0$= 9 g/h, pH = 7, T = 180 min	phenylarsonic 13.4×10^3	99.6%	----	0.6
6	photolysis[6]	UV 500 W, λ = 365 nm, pH_0 = 4.3, V = 40 mL, T = 180 min	4-amino phenyl -arsenic acid 92	87%	----	0.006
7	UV/$S_2O_8^{2-}$[13]	UV 6 W, λ = 254 nm, $[S_2O_8^{2-}]_0$ = 1000 μM, pH = 3.0, V = 250 mL	MMA, 100	99.4%, T = 21 min	----	0.887;
			DMA, 100	96.7%, T = 35 min	----	1.036

DOI: 10.1021/acs.iecr.5b01012
Ind. Eng. Chem. Res. 2015, 54, 8277−8286

Research of China (No. 2011CB605703 and No. 14CX06117A).

REFERENCES

(1) Andjelkovic, I.; Stankovic, D.; Nesic, J.; Krstic, J.; Vulic, P.; Manojlovic, D.; Roglic, G. Fe Doped TiO_2 Prepared by Microwave-Assisted Hydrothermal Process for Removal of As(III) and As(V) from Water. *Ind. Eng. Chem. Res.* **2014**, *53*, 10841.

(2) Czaplicka, M.; Bratek, U.; Jaworek, K.; Bonarski, J.; Pawlak, S. Photo-oxidation of p-arsanilic acid in acidic solutions: Kinetics and the identification of by-products and reaction pathways. *Chem. Eng. J.* **2014**, *243*, 364.

(3) Dominguez-Ramos, A.; Chavan, K.; García, V.; Jimeno, G.; Albo, J.; Marathe, K. V.; Yadav, G. D.; Irabien, A. Arsenic Removal from Natural Waters by Adsorption or Ion Exchange: An Environmental Sustainability Assessment. *Ind. Eng. Chem. Res.* **2014**, *53*, 18920.

(4) Garbarino, J. R.; Bednar, A. J.; Rutherford, D. W.; Beyer, R. S.; Wershaw, R. L. Environmental fate of roxarsone in poultry litter. I. Degradation of roxarsone during composting. *Environ. Sci. Technol.* **2003**, *37*, 1509.

(5) Adak, A.; Mangalgiri, K. P.; Lee, J.; Blaney, L. UV irradiation and UV-H_2O_2 advanced oxidation of the roxarsone and nitarsone organoarsenicals. *Water Res.* **2014**, *70*, 74.

(6) Zhu, X. D.; Wang, Y. J.; Liu, C.; Qin, W. X.; Zhou, D. M. Kinetics, intermediates and acute toxicity of arsanilic acid photolysis. *Chemosphere* **2014**, *107*, 274.

(7) Stolz, J. F.; Perera, E.; Kilonzo, B.; Kail, B.; Crable, B.; Fisher, E.; Ranganathan, M.; Wormer, L.; Basu, P. Biotransformation of 3-Nitro-4-hydroxybenzene Arsonic Acid and Release of Inorganic Arsenic by Clostridium Species. *Environ. Sci. Technol.* **2007**, *41*, 818.

(8) Vu, K. B.; Kaminski, M. D.; Nunez, L.; Vu, K. B.; Nunez, L. *Review of arsenic removal technologies for contaminated groundwaters*. Report No. ANL-CMT-03/2; Argonne National Laboratory: Argonne, Illinois, 2003

(9) Sorlini, S.; Gialdini, F. Conventional oxidation treatments for the removal of arsenic with chlorine dioxide, hypochlorite, potassium permanganate and monochloramine. *Water Res.* **2010**, *44*, 5653.

(10) Hug, S. J.; Leupin, O. Iron-catalyzed oxidation of arsenic(III) by oxygen and by hydrogen peroxide: pH-dependent formation of oxidants in the Fenton reaction. *Environ. Sci. Technol.* **2003**, *37*, 2734.

(11) Emett, M. T.; Khoe, G. H. Photochemical oxidation of arsenic by oxygen and iron in acidic solutions. *Water Res.* **2001**, *35*, 649.

(12) Jaworek, K.; Czaplicka, M.; Bratek, L. Decomposition of phenylarsonic acid by AOP processes: degradation rate constants and by-products. *Environ. Sci. Pollut. Res.* **2014**, *21*, 11917.

(13) Yoon, S. H.; Lee, S.; Kim, T. H.; Lee, M.; Yu, S. Oxidation of methylated arsenic species by UV/$S_2O_8^{2-}$. *Chem. Eng. J.* **2011**, *173*, 290.

(14) Zheng, S.; Jiang, W.; Cai, Y.; Dionysiou, D. D.; O'Shea, K. E. Adsorption and photocatalytic degradation of aromatic organoarsenic compounds in TiO_2 suspension. *Catal. Today* **2014**, *224*, 83.

(15) Jiang, B.; Zheng, J.; Qiu, S.; Wu, M. B.; Zhang, Q.; Yan, Z.; Xue, Q. Review on electrical discharge plasma technology for wastewater remediation. *Chem. Eng. J.* **2014**, *236*, 348.

(16) Reddy, P. M. K.; Subrahmanyam, C. Green Approach for Wastewater Treatment—Degradation and Mineralization of Aqueous Organic Pollutants by Discharge Plasma. *Ind. Eng. Chem. Res.* **2012**, *51*, 11097.

(17) Jiang, B.; Guo, J.; Wang, Z.; Zheng, X.; Zheng, J.; Wu, W.; Wu, M.; Xue, Q. A green approach towards simultaneous remediations of chromium(VI) and arsenic(III) in aqueous solution. *Chem. Eng. J.* **2015**, *262*, 1144.

(18) Jiang, B.; Hu, P.; Zheng, X.; Zheng, J.; Tan, M.; Wu, M.; Xue, Q. Rapid oxidation and immobilization of arsenic by contact glow discharge plasma in acidic solution. *Chemosphere* **2015**, *125*, 220.

(19) Paktunc, D.; Bruggeman, K. Solubility of nanocrystalline scorodite and amorphous ferric arsenate: Implications for stabilization of arsenic in mine wastes. *Appl. Geochem.* **2010**, *25*, 674.

(20) Dhar, R. K.; Zheng, Y.; Rubenstone, J.; vanGeen, A. A rapid colorimetric method for measuring arsenic concentrations in groundwater. *Anal. Chim. Acta* **2004**, *526*, 203.

(21) Liu, R.; Guo, Y.; Wang, Z.; Liu, J. Iron species in layered clay: efficient electron shuttles for simultaneous conversion of dyes and Cr(VI). *Chemosphere* **2014**, *95*, 643.

(22) Eisenberg, G. Colorimetric Determination of Hydrogen Peroxide. *Ind. Eng. Chem., Anal. Ed.* **1943**, *15*, 327.

(23) Ishibashi, K.; Fujishima, A.; Watanabe, T.; Hashimoto, K. Detection of active oxidative species in TiO_2 photocatalysis using the fluorescence technique. *Electrochem. Commun.* **2000**, *2*, 207.

(24) Han, W.; Zhu, W.; Zhang, P.; Zhang, Y.; Li, L. Photocatalytic degradation of phenols in aqueous solution under irradiation of 254 and 185 nm UV light. *Catal. Today* **2004**, *90*, 319.

(25) Gai, K. Plasma-induced degradation of diphenylamine in aqueous solution. *J. Hazard. Mater.* **2007**, *146*, 249.

(26) Xu, T.; Kamat, P. V.; Joshi, S.; Mebel, A. M.; Cai, Y.; O'Shea, K. E. Hydroxyl radical mediated degradation of phenylarsonic acid. *J. Phys. Chem. A* **2007**, *111*, 7819.

(27) Wang, Z.; Bush, R. T.; Sullivan, L. A.; Chen, C.; Liu, J. Selective oxidation of arsenite by peroxymonosulfate with high utilization efficiency of oxidant. *Environ. Sci. Technol.* **2014**, *48*, 3978.

(28) Roots, R.; Okada, S. Estimation of life times and diffusion distances of radicals involved in X-ray-induced DNA strand breaks of killing of mammalian cells. *Radiat. Res.* **1975**, *64*, 306.

(29) De Klerk, R. J.; Jia, Y.; Daenzer, R.; Gomez, M. A.; Demopoulos, G. P. Continuous circuit coprecipitation of arsenic(V) with ferric iron by lime neutralization: Process parameter effects on arsenic removal and precipitate quality. *Hydrometallurgy* **2011**, *111-112*, 65.

(30) Song, S.; Lopez-Valdivieso, A.; Hernandez-Campos, D. J.; Peng, C.; Monroy-Fernandez, M. G.; Razo-Soto, I. Arsenic removal from high-arsenic water by enhanced coagulation with ferric ions and coarse calcite. *Water Res.* **2006**, *40*, 364.

(31) Tokoro, C.; Yatsugi, Y.; Koga, H.; Owada, S. Sorption Mechanisms of Arsenate during Coprecipitation with Ferrihydrite in Aqueous Solution. *Environ. Sci. Technol.* **2009**, *44*, 638.

(32) Demopoulos, G. P. Aqueous precipitation and crystallization for the production of particulate solids with desired properties. *Hydrometallurgy* **2009**, *96*, 199.

(33) Bang, S.; Johnson, M. D.; Korfiatis, G. P.; Meng, X. Chemical reactions between arsenic and zero-valent iron in water. *Water Res.* **2005**, *39*, 763.

(34) Lu, P.; Zhu, C. Arsenic Eh−pH diagrams at 25°C and 1bar. *Environ. Earth Sci.* **2011**, *62*, 1673.

(35) Buxton, G. V.; Greenstock, C. L.; Helman, W. P.; Ross, A. B.; Tsang, W. Critical Review of rate constants for reactions of hydrated electrons, hydrogen atoms and hydroxyl radicals in Aqueous Solution. *J. Phys. Chem. Ref. Data* **1988**, *17*, 513.

(36) Paktunc, D.; Bruggeman, K. Solubility of nanocrystalline scorodite and amorphous ferric arsenate: Implications for stabilization of arsenic in mine wastes. *Appl. Geochem.* **2010**, *25*, 674.

(37) Zhao, X.; Zhang, B.; Liu, H.; Qu, J. Removal of arsenite by simultaneous electro-oxidation and electro-coagulation process. *J. Hazard. Mater.* **2010**, *184*, 472.

(38) Raven, K. P.; Jain, A.; Loeppert, R. H. Arsenite and Arsenate Adsorption on Ferrihydrite: Kinetics, Equilibrium, and Adsorption Envelopes. *Environ. Sci. Technol.* **1998**, *32*, 344.

(39) Goldberg, S.; Johnston, C. T. Mechanisms of Arsenic Adsorption on Amorphous Oxides Evaluated Using Macroscopic Measurements, Vibrational Spectroscopy, and Surface Complexation Modeling. *J. Colloid Interface Sci.* **2001**, *234*, 204.

(40) Zhang, Y.; Yang, M.; Dou, X. M.; He, H.; Wang, D. S. Arsenate Adsorption on an Fe-Ce Bimetal Oxide Adsorbent: Role of Surface Properties. *Environ. Sci. Technol.* **2005**, *39*, 7246.

(41) Harvey, D. T.; Linton, R. W. Chemical characterization of hydrous ferric oxides by X-ray photoelectron spectroscopy. *Anal. Chem.* **1981**, *53*, 1684.

(42) Yamashita, T.; Hayes, P. Analysis of XPS spectra of Fe^{2+} and Fe^{3+} ions in oxide materials. *Appl. Surf. Sci.* **2008**, *254*, 2441.

DOI: 10.1021/acs.iecr.5b01012
Ind. Eng. Chem. Res. 2015, 54, 8277−8286

(43) Zhang, G. S.; Qu, J. H.; Liu, H. J.; Liu, R. P.; Li, G. T. Removal mechanism of As(III) by a novel Fe-Mn binary oxide adsorbent: oxidation and sorption. *Environ. Sci. Technol.* **2007**, *41*, 4613.
(44) Lu, D.; Ji, F.; Wang, W.; Yuan, S.; Hu, Z. H.; Chen, T. Adsorption and photocatalytic decomposition of roxarsone by TiO_2 and its mechanism. *Environ. Sci. Pollut. Res.* **2014**, *21*, 8025.

DOI: 10.1021/acs.iecr.5b01012
Ind. Eng. Chem. Res. 2015, 54, 8277−8286